ADVANCED ENERGY MATERIALS
www.advenergymat.de

Lithium Borate Ionic Liquids as Single-Component Electrolytes for Batteries

*Gregorio Guzmán-González, Marta Alvarez-Tirado, Jorge L. Olmedo-Martínez, Matías L. Picchio, Nerea Casado, Maria Forsyth, and David Mecerreyes**

Current electrolytes for lithium batteries are usually composed of at least two chemical compounds, an organic solvent such as a cyclic carbonate and a lithium salt such as $LiPF_6$. Here, the concept of using a single-component electrolyte is demonstrated in lithium batteries based on new lithium borate ionic liquids at room temperature. The design concept of this class of lithium ionic liquids (LiILs) is based on an asymmetrically substituted central tetra-coordinate boron atom with oligoethylene glycol groups, fluorinated electron-attracting groups, and one alkane group. The optimized borate—Li^+ LiILs show a high ionic conductivity value of $>10^{-4}$ S cm^{-1} at 25 °C, high lithium transference numbers (t_{Li^+} = 0.4 – 0.5) and electrochemical stability (>4 V). Some of the LiILs present high compatibility with lithium-metal electrodes showing stable polarization profiles in platting/stripping tests. The selected LiIL is investigated as single-component electrolytes in lithium-metal battery cells showing discharge capacity values in Li^0/LiIL/lithium–iron phosphate and Li^0/LiIL/lithium titanate cells of 124 and 75 mAh g^{-1}, respectively, at a C-rate of 0.2 C and 65 °C with low-capacity loss.

1. Introduction

Among all energy storage devices, lithium-ion batteries (LIBs) show outstanding specific gravimetric and volumetric charge capacities that give them versatility for use in a wide variety of mobile electronic devices.[1] Most current commercial LIBs use liquid electrolytes, which consist of lithium-ion salts dissolved in a solvent or mixture of them (usually organic carbonates). As a drawback, the generation of concentration gradients derived from anionic polarization is a factor that controls and limits the electrochemical performance of LIBs, mainly at high current density values.[2,3]

To prevent and decrease the overpotential generated by salt concentration polarization, one popular strategy is the immobilization of anions by attaching them to a polymer matrix.[4] However, the overall ionic conductivity of the so-called single lithium-ion polymer electrolytes (SLICPE) is often severely affected by the decrease in the number of mobile ions and their transport through the polymer matrix.[3,5] This is coupled with the intrinsic complexity of establishing a proper solid–solid contact between the SLICPE/electrode interface,[4] which often requires the use of additives to improve the wettability properties necessary for operation under real conditions. Another common practice for the prevention of salt concentration polarization in electrolytes for LIBs is the decrease or elimination of solvent in liquid electrolytes, either by preparing highly concentrated electrolytes or by preparing electrolytes based on ionic liquids (in which the anions and cations of the ILs behave as a solvent for the lithium salts).[6,7] However, in both cases, all the problems associated with polarization by lithium salt concentration gradients in the electrolyte persist, because prevention of this type of polarization in the electrolyte requires strict solvent removal and Li^+ to be the only latently mobile cation in the system.[8] This reasoning inspired the development of some room-temperature (RT) lithium ionic liquids (LiILs) for use as solvent-free liquid electrolytes.[9] However, up to now, the reported LiILs were only used as additives or salts in common multicomponent organic solvent electrolytes.[10,11]

The first type of LiILs was reported by Fujinami and Buzoujima,[12] which consists of a variety of lithium aluminates containing two oligoether groups and two electron-withdrawing groups. Watanabe and co-workers[13] subsequently presented a new family of LiILs with similar geometry, changing the central aluminum atom to a boron atom designed to decrease the basicity of the anionic aluminate center. This substitution diminishes the interaction energy with Li^+ and promotes the ionic mobility of the salts. Langwald and co-workers explored extensively different synthesis routes to obtain some new LiILs families, specifically difluoro alkoxy boranes and trialkyl borates, whose oxyethylene substituents are of different lengths and different

G. Guzmán-González,[+] M. Alvarez-Tirado, J. L. Olmedo-Martínez, M. L. Picchio, N. Casado, M. Forsyth, D. Mecerreyes
POLYMAT
University of the Basque Country UPV/EHU Joxe Mari Korta Center
200018 Donostia-San Sebastián, Spain
E-mail: david.mecerreyes@ehu.es

N. Casado, M. Forsyth, D. Mecerreyes
IKERBASQUE
Basque Foundation for Science
48013 Bilbao, Spain

M. Forsyth
Institute for Frontier Materials (IFM)
Deakin University
Burwood Victoria 3125, Australia

The ORCID identification number(s) for the author(s) of this article can be found under https://doi.org/10.1002/aenm.202202974.

[+]Present address: Departamento de Química, Universidad Autónoma Metropolitana-Iztapalapa, 09340, México City, México

DOI: 10.1002/aenm.202202974

electron-withdrawing groups.[14–16] Those substituents were able to modulate and determine that the Li^+/ethoxy groups (Li^+/EO) ratio, which provides the best ionic transport conditions in LiILs, is based on boron atoms as anionic centers substituted with one and three methoxy polyethylene glycol chains showing ionic conductivity values as high as 7.2×10^{-5} and 3.2×10^{-5} S cm^{-1} at 30 °C, respectively. Thus, it can be deduced that for this type of LiILs, between 7 and 9 ethylene glycol units in the oligomer chains are necessary to achieve efficient dissolution of the borate—Li^+ complex without affecting the ionic conductivity by decreasing the Li^+ concentration in the system. However, this ratio can be slightly modified by particular characteristics of the substituent groups, such as size and electron-withdrawing capacity. On the other hand, DesMarteau and co-workers[9,17] reported another new type of lithium liquid salts consisting of lithium (perfluoro vinyl ether) sulfonimide salts covalently bonded to an oxyethylene chain with different lengths of the solvating lithium ethoxy chain, which possessed high thermal stability. Analysis of the ionic transport properties of these types of salts showed that the highest values of ionic conductivity 4.1×10^{-6} S cm^{-1} at 30 °C were found in the lithium (perfluoro vinyl ether) sulfonimide salts, which maintain a Li^+/EO ratio of 11.2. The decrease of the Li^+ concentration in the system due to the increase of the amount of EO groups necessary to solvate the lithium sulfonimide complex, for the borate—Li^+ complexes described above, could be one of the main factors affecting the ionic mobility of these systems. On the other hand, the ionic conductivity values (6.5×10^{-7} S cm^{-1} at 30 °C) found for the triethylene glycol-based 1,2,3-triazolate lithium LiILs reported by Drockenmuller and co-workers[18] seemed to be limited by a poor concentration of EO groups in the system (Li^+/EO ratio = 3), insufficient to dissociate the ionic couple, especially at low temperatures. However, although the concept of lithium liquid ionic liquids was demonstrated in these works, they have not shown the necessary electrochemical characteristics as single-component electrolytes for lithium batteries (**Figure 1**).

In this article, we report on a new family of LiIL salts and the proof of concept of their use as monocomponent electrolytes in batteries. The LiILs were synthesized using the previously reported methodology for obtaining lithium borate salts from the simple reaction between trialkoxy borates with *n*-butyl lithium.[5] We synthesized a series of new lithium ionic liquids with highly delocalized anionic groups based on tetracoordinate borate groups asymmetrically coordinated by two oxyethylene chains ($-O(CH_2CH_2O)_3CH_3$), a variable electron-withdrawing group ($-OR^F$) that modifies the electron density of the anionic center and its interaction energy with Li^+,[15,19] and an alkane substituent linked by a boron—carbon covalent bond ($-CR^C$). The alkane substituent was derived from the addition of organolithium compounds, which stabilize, decrease the hygroscopicity of the anionic center, and supply Li^+ for the borate complexe formation.[5,20] By designing 11 different LiILs, we investigated the effect of various substituents in the intrinsic electrochemical properties such as ionic conductivity, lithium transference number, and electrochemical stability window. Finally, it was demonstrated that the LiILs reported here possess the necessary lithium platting–stripping ability and could be used as single-component electrolytes for lithium batteries showing good performance and cyclability with well-known electrode materials.

2. Results and Discussion

2.1. Synthesis and Structural Characterization of LiILs

The LiILs were synthesized according to the general synthetic scheme (**Figure 2**a). In the first step, trialkoxy borates were synthesized by reacting two equivalents of ethylene glycols and fluorinated alcohols stepwise with boron trihydride. In the second step, the trialkoxy borates were reacted with an organolithium compound to yield the LiILs in high conversions (>90%). Using this methodology, different LiILs were designed combining different substituents as shown in Figure 2b. As fluorinated alcohols ($H-OR^F$) we investigated LiILs based on 2,2,2-trifluoroethanol (3FE), 1,1,1,3,3,3-hexafluoro-2-propanol (6FiP), 1,1,1,3,3,3-hexafluoro-2-trifluoromethyl-2-propanol (9FMtB), 1,1,3, 3,3-hexafluoro-2-methyl-2-propanol (6FMtB), 2-trifluoromethyl-2-propanol (3FMtB), and 1,1,1-trifluoro-2-propanol (3FMiP). Then as organolithium compounds, we used *n*-butyl lithium as well as *sec*-butyl lithium, *ter*-butyl lithium, methyl lithium, and phenyl lithium. The experimental procedures and the structural characterization are presented in detail in the "Experimental Section" of the Supporting Information.

The NMR spectra obtained for the LiIL2, LiIL7, LiIL8, LiIL9, and LiIL10 present a series of characteristic signals due to their similar substituents with the exception of the alkane signals. The ^{11}B NMR spectra collected for the LiILs of the R^C-LLS2 form revealed that in solution there were boron atoms with two different types of coordination (**Figure 3**). The main peaks in the range of δ = 2.78–4.78 ppm referred to tetrahedral boron in monochelate complexes and are associated with obtaining the main products according to the proposed reaction (Figure 2a). The peak in the range of δ = 1.98–2.78 ppm is associated with the formation of tetracoordinate complexes with different distribution of $-OR^F$ or methoxy polyethylene glycol groups substituted on the central boron atom, favored by the thermodynamic equilibrium of the reaction, which was determined by the ratio of reactants and the conditions of synthesis of the trialkoxy borates. The broad peak located in the range of δ = 6.1–9.2 ppm, more evident in LiIL2 and LiIL10 electrolytes, was associated with the presence of free borate anions (anions not complexed with Li^+, derived from the solvation process of LiIL). Particularly, for LiIL9 and LiIL10 electrolytes, the peaks in the range of δ = 18–23 ppm were due to the tricoordinate boron atoms, which corresponded to the trialkoxy borates not chelated in the second stage of the proposed synthesis scheme, due to kinetic and/or thermodynamic limitations. The ratio of B^4/B^3 was 0.89/0.11, indicating that the methyl lithium and phenyl lithium compounds offer lower efficiency in the chelation reaction.

2.2. Ionic Conductivity of LiILs

First we analyzed the effect of the modification of the electronic density of the borate groups on ionic conductivity (**Figure 4**a). The structural modifications of the LiILs associated with the size of the substituents should determine their intrinsic properties such as viscosity, density, Li^+ concentration, ionic conductivity, and electrochemical stability. Interestingly, all the synthesized asymmetric LiILs presented a significant increase in their ionic conductivity values relative to the previously

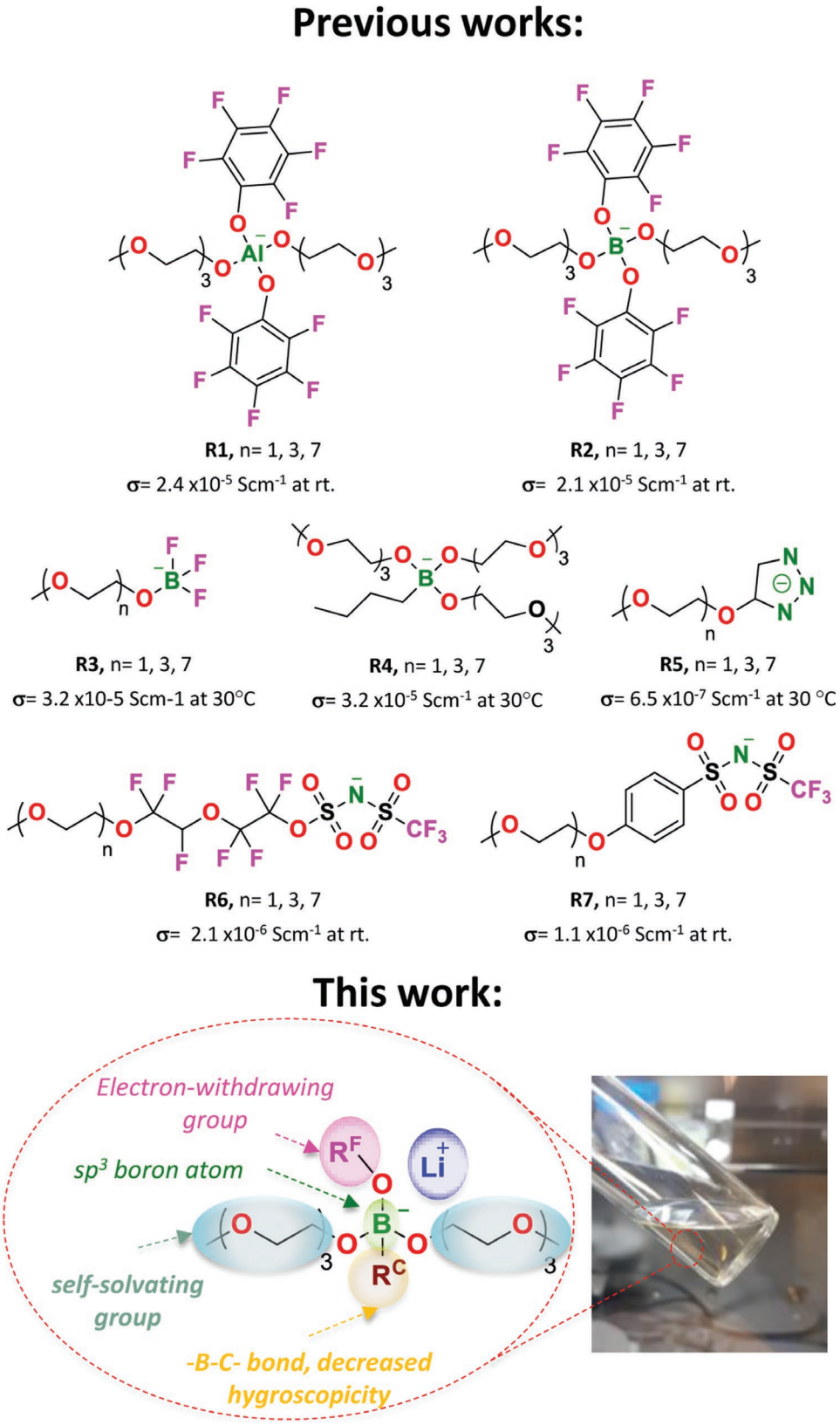

Figure 1. Molecular structures of reported lithium ionic liquids (LiILs).

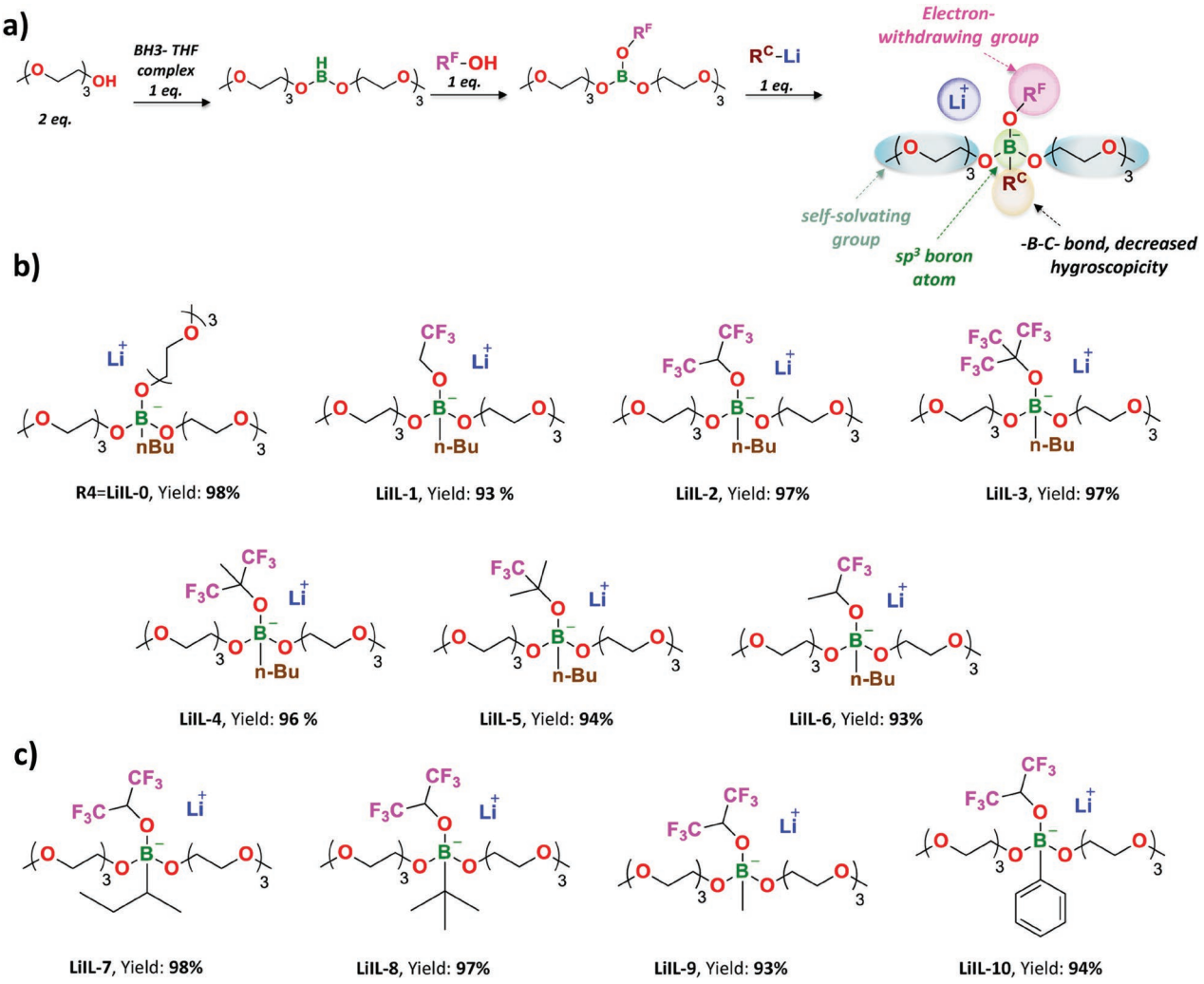

Figure 2. Lithium ionic liquid (LiILs). a) Synthetic route for lithium ionic liquids (LiILs). b) Synthetized LiIL molecules showing different electron-withdrawing substituent. c) Different alkane stabilizing group substituent of the borate—Li^+ complex.

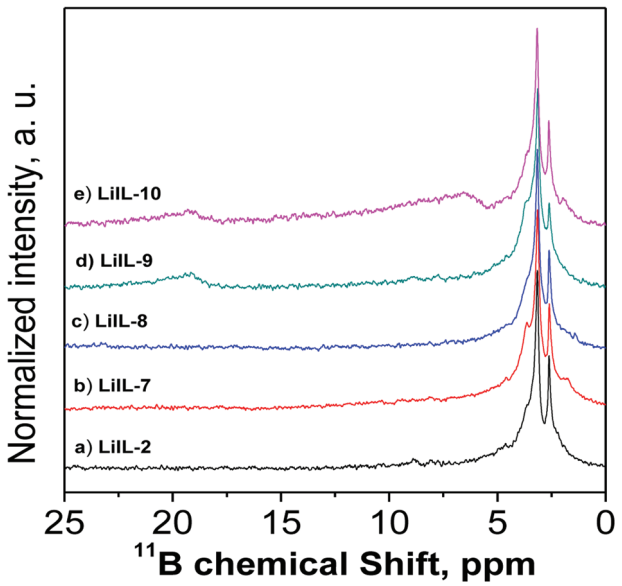

Figure 3. ^{11}B NMR in CDCl3 dissolution for R^C—LiILs electrolytes.

reported symmetric LiIL0 electrolyte. This could be due to the decrease in the interaction energy of the borate—Li^+ complex generated by the increased delocalization of the negative charge in the anionic center, mainly due to the substitution of one of the glycol groups by the fluorinated groups.

LiIL1 having a trifluoroethanoxy substituent is the simplest of the LiILs proposed from a structural point of view. The ionic conductivity values obtained for the LiLL0 and LiIL1 electrolytes, 5.29×10^{-6} and 4.39×10^{-5} S cm^{-1} at RT, respectively, could explain the role of the electron-withdrawing strength of the fluorinated substituent, on the decrease of the electron density of the anionic center and its interaction energy with Li^+.[21] The secondary hexafluoro-2-propanoxy substituent as an electron-withdrawing ligand in the LiIL2 electrolyte allows a further decrease in the electron density of its anionic center. This facilitates ion dissociation and favors ionic mobility, which was directly reflected in its increased ionic conductivity values of 1.14×10^{-4} S cm^{-1} at 25 °C. However, this trend was broken by the LiIL3 electrolyte. Regardless of possessing a lower activation energy for the ionic conduction process relative to LiIL1 and LiIL2 electrolytes (**Table 1**), LiIL3 exhibited

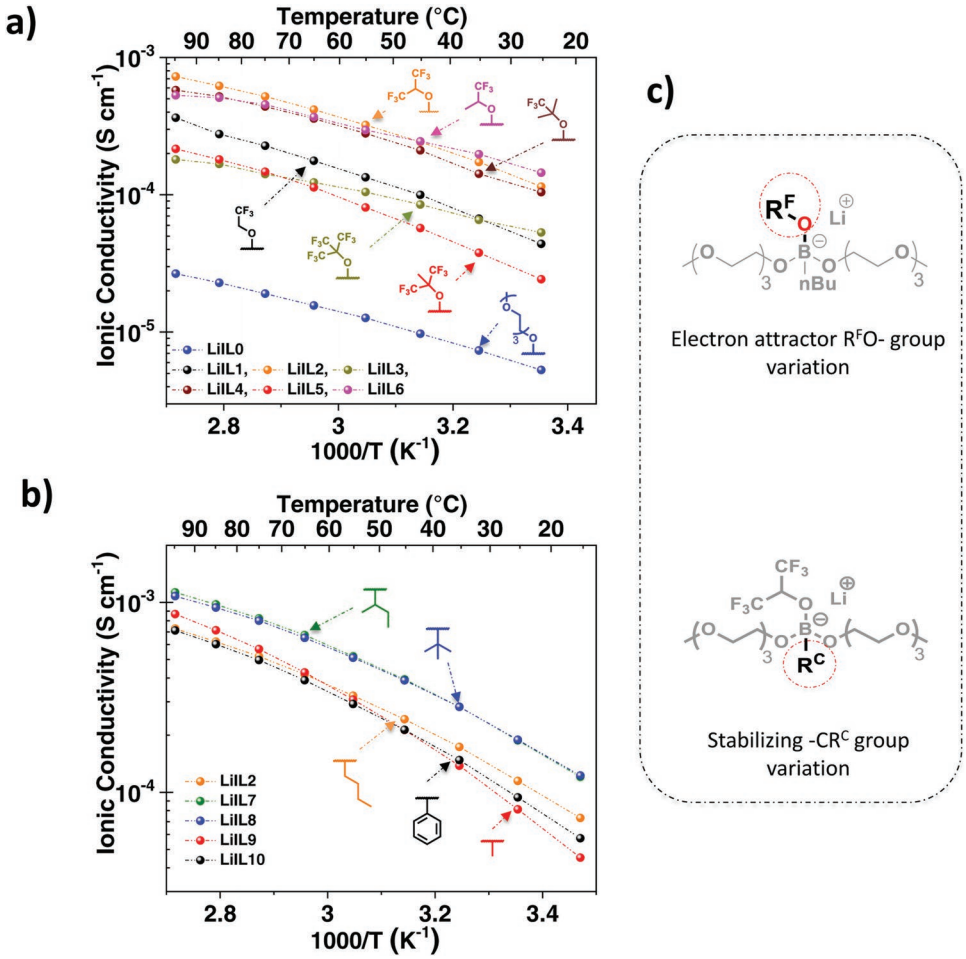

Figure 4. Temperature dependence of ionic conductivity for LiILs. a) Effect of the electron attractor R^FO- group variation. b) Effect of the stabilizing group $-CR^C$ variation. c) Molecular structures denoting the basis of each of the LiILs groups highlighting the variable functional group in each case.

lower ionic conductivity values of 5.31×10^{-5} S cm^{-1} (in particular, at high temperatures). This could indicate that the use of the ternary hexafluoro-2-trifluoromethyl-2-propanoxy as an electron-withdrawing substituent results in the formation of negatively charged parts/fragments in the anion structure that are attractive for Li^+ interaction, which limited the dissociation of the borate—Li^+ complex, and decreases ion mobility.[22,23]

Table 1. Summary of ionic transport properties for synthesized LiILs.

	σ at 25 °C S cm^{-1}	E_a [eV]	t_{Li^+}
LiIL-0	5.30×10^{-06}	0.066	0.44
LiIL-1	4.39×10^{-05}	0.121	0.36
LiIL-2	1.15×10^{-04}	0.108	0.42
LiIL-3	5.32×10^{-05}	0.074	0.56
LiIL-4	1.04×10^{-04}	0.103	0.45
LiIL-5	2.43×10^{-05}	0.130	0.43
LiIL-6	1.45×10^{-04}	0.116	0.51
LiIL-7	1.87×10^{-04}	0.113	0.43
LiIL-8	1.89×10^{-04}	0.110	0.45
LiIL-9	8.13×10^{-05}	0.148	0.51
LiIL-10	9.40×10^{-05}	0.127	0.47

The LiIL4 electrolyte confirmed that the incorporation of the ternary hexafluoro-2-methyl-2-propanoxy as an electron-withdrawing substituent lowered the activation energy and yielded higher ionic conductivity values as high as 1.04×10^{-4} S cm^{-1} at 25 °C, which were comparable with those obtained for LiIL2. The LiIL5 derived from the ternary alcohol 2-trifluoromethyl-2-propanol, having only one equal amount of CF_3 groups in the electron-withdrawing substituent, shows a low ionic conductivity value of 2.43×10^{-5} S cm^{-1}. In contrast, LiIL6 electrolyte, derived from the secondary trifluoro-2-propanoxy, exhibited ionic conductivity values that are among the highest obtained in this first stage for LiILs, being 1.44×10^{-4} S cm^{-1} at 25 °C.

Based on the above, we can appreciate that the level of electronic delocalization in the LiIL2 and LiIL4 electrolytes with two $-CF_3$ groups in the electron-withdrawing ligand and the size of the molecular structure of the substituents in the LiIL2 and LiIL6 electrolytes derived from secondary alkoxy substituents offered the highest ionic conductivity values. Thus, it is possible to conclude that the effect into the electronic delocalization generated by the hexafluoro-2-methyl-2-propanol ligand in the LiIL2 electrolyte seemed to be the most appropriate since it guaranteed a fair distribution of the

negative charge density between the anionic center and the ligands; avoiding the risk of the formation of negatively charged parts/fragments attractive for the interaction of the lithium ion could affect the dissociation of the borate—Li^+ complex.

Next, the effect of the nature of the organolithium groups (—CR^c) used as the lithium and alkane substituent precursor and stabilizing groups for the formation of R^C—LiILs on the ionic conductivity was investigated. Figure 4b shows that the different structural configurations of the butyl groups as substituents in R^C—LLS2 had a considerable effect on the ionic conductivity of the LiILs. As expected, the *n*-butyl group in the LiIL2 electrolyte with the highest number of hydrogen atoms on the α-carbon generates the lowest electronic delocalization, which is reflected in its ionic conductivity value of 1.14×10^{-4} S cm^{-1} at 25 °C. On the other hand, the use of *sec*-butyl and *ter*-butyl groups decreased the number of hydrogen atoms on the α-carbon thereby increasing the electronic delocalization and the ionic mobility. However, based on the ionic conductivity values obtained for LiIL7 and LiIL8 electrolytes, it is not possible to appreciate a significant difference. This is likely due to the balance between the electron-withdrawing capacity and the steric hindrance generated by their structural conformation.

On the other hand, the substitution of the butyl groups by a relatively smaller group, such as methyl, in the LiIL9 electrolyte did not provoke an increase in its ionic conductivity values. This negative effect is probably due to the strong interaction between the methyl group and Li^+ generated by the high electron density of its hydrogen atoms. Similar behavior was found for the LiIL10 electrolyte, for which the high electron-withdrawing capacity generated by the incorporation of the phenyl group promoted charge delocalization at the anionic center and weakened its interaction with Li^+. However, together with the increase of the anion size, the strong interaction of Li^+ with the π-bonds of the phenyl group becomes the main limiting factor in the borate—Li^+ complex dissociation, as shown by the relatively low values of ionic conductivity obtained.

The ionic conductivity of LiILs can be correlated with other intrinsic properties such as viscosity, which generally decreases with increasing temperature (Figure S2, Supporting Information), i.e., an inverse behavior to that presented during ionic conductivity measurements. Usually, these two properties are correlated through the Walden diagram, as it allows an easy classification of ionic liquids based on its ionicity (**Figure 5**). The line of ideality is determined by dilute KCl solution, and we note that Walden's rules are only applicable to infinitely dilute electrolyte solutions, where the different ionic species in the liquid are independent of each other without interaction. However, the Walden diagram showed before excellent applicability to ILs and served as a guide for their classification and selection. Based on this classification,[24,25] it is possible to affirm that all LiILs synthesized and evaluated in this work present a typical behavior of good liquid ions since they maintain a good relationship between flux and ionic mobility since the effect of van der Waals forces on ion–ion interactions is relatively low.[26]

The lithium transference number (t_{Li^+}) for the synthesized LiILs was determined by the alternating current (AC)–direct current (DC) polarization experiment according to the Evans–Bruce protocol,[27] and reported in Table 1 (see example in Figure S1 of Supporting Information). The LiILs reported here showed relatively high lithium transference numbers for liquid

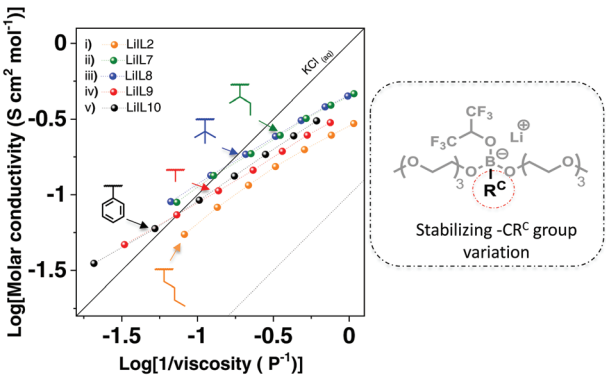

Figure 5. Walden plot for selected R^C—LiILs.

electrolytes showing values between 0.4 and 0.6. Particularly, for the LiILs with higher ionic conductivity values LiIL2, LiIL4, and LiIL6, the t_{Li^+} showed high values of 0.42, 0.45, and 0.47, respectively. These molecules were therefore selected as the best LiILs to be further investigated in electrochemical cells.

2.3. Electrochemical Stability Window of LiILs

The linear sweep voltammograms (LSV) for LiILs are shown in Figure S3a (Supporting Information). The most pronounced oxidation of LiIL2, LiIL7, and LiIL8 electrolytes was identified by a drastic increase of the anodic currents, at potentials of 4.7, 4.9, and 5.2 V versus Li^0/Li^+, respectively, corresponding to the coexisting oxidation of their ethylene glycol chains and anionic centers.[21,22] The trend of these subsequent increases in electrochemical stability values for LiILs; LiIL2, LiIL7, and LiIL8 are attributed to increased delocalization of the negative charge at the anionic centers, which provides the borate anion with increased resistance to oxidation reactions.[28,29]

Similar behavior was presented by LiIL9 and LiIL10 electrolytes, where the current profiles did not seem to show the typical exponential increase of current indicating their oxidation potential (Figure S3a, Supporting Information). All in all, small anodic currents (<0.2 μA cm^{-2}) at 3.7 V versus Li^0/Li^+ associated with the slow onset of oxidative chain decompositions of the ethylene glycol chains were observed in all R^C—LiIL electrolytes as shown in the inset of Figure S3a (Supporting Information).[30] Consequently, it could be assumed that the LiILs prepared in this work could be used as electrolytes in cells with electrode materials working at a potential of <3.8 V versus Li^0/Li^+, such as lithium–iron phosphate (LFP) or lithium titanate (LTO).

A series of cyclic voltammetries were performed for LiIL2, LiIL7, and LiIL8 electrolytes measured in Li^0/R^C—LiIL/copper cells at 40 °C. As shown in Figure S3b (Supporting Information), in the open circuit potential range at –0.5 V versus Li^0/Li^+ in the initial sweep, no minor peaks were observed that could be associated with secondary reactions including decomposition of borate anion and/or R^C—LLS2 impurities. In the subsequent CV cycles (Figure S3b, Supporting Information), for the lithium plating/stripping processes located in the range from –0.5 to 0.2 V versus Li^0/Li^+, an increase of the average Coulombic efficiency (CE) is observed during the first

few cycles. This was expected since the electrochemical anion reduction generates robust and relatively stable solid electrolyte interphase layers on the lithium-metal electrode.

2.4. Interfacial Stability of LiILs with Lithium-Metal Electrode

Many authors have studied the growth of dendrites on electrodes, and it has been determined that this is one of the main factors affecting the electrochemical performance and lifetime of lithium-metal batteries. Therefore, it was carried out this test to evaluate the performance of all types of electrolytes, which is their compatibility with lithium-metal electrodes.

Unlike other electrolyte systems that involve mixing ionic liquids with lithium salts to enhance salt dissociation and promote ionic conductivity and compatibility at the electrode–electrolyte interface,[31,32] the LiILs synthesized in this work were evaluated as single-competent electrolytes to assess their intrinsic properties. The evaluation of the interfacial stability of the LiILs was performed in two stages: the first stage consisted of determining the critical current density (CCD) for the *n*-LiIL2, LiIL7, and LiIL8 electrolytes selected for showing the best ionic conductivity and electrochemical stability characteristics. The polarization profiles for the $Li^0/LiILs/Li^0$ symmetrical cells assembled with the selected electrolytes were evaluated at consecutive current rates of ±0.01, ±0.1, ±0.2, ±0.5, and ±0.8 mA cm^{-2} at 45 °C. For each current density, the cells were subjected to five cycles (2 h per cycle).

As expected, the $Li^0/LiILs/Li^0$ cells assembled present similar polarization profiles (Figure S4, Supporting Information); consequently, a single CCD value of ±0.2 mA cm^{-2} at 45 °C was determined obtaining overpotential values of <0.45 V versus Li^0/Li^+. LiILs were considered inoperable in $Li^0/LiIL/Li^0$ symmetrical cells at applied current density values > ±0.5 mA cm^{-2} at 45 °C as they generated overpotential values of >±1 V versus Li^0/Li^+. To analyze the stability and compatibility of different R^C—LiIL electrolytes with lithium metal, Li^0/R^C—LLS2/Li^0 symmetrical cells were assembled. The long-term cycling stability at a current density of 0.2 mA cm^{-2} is shown in **Figure 6**. The

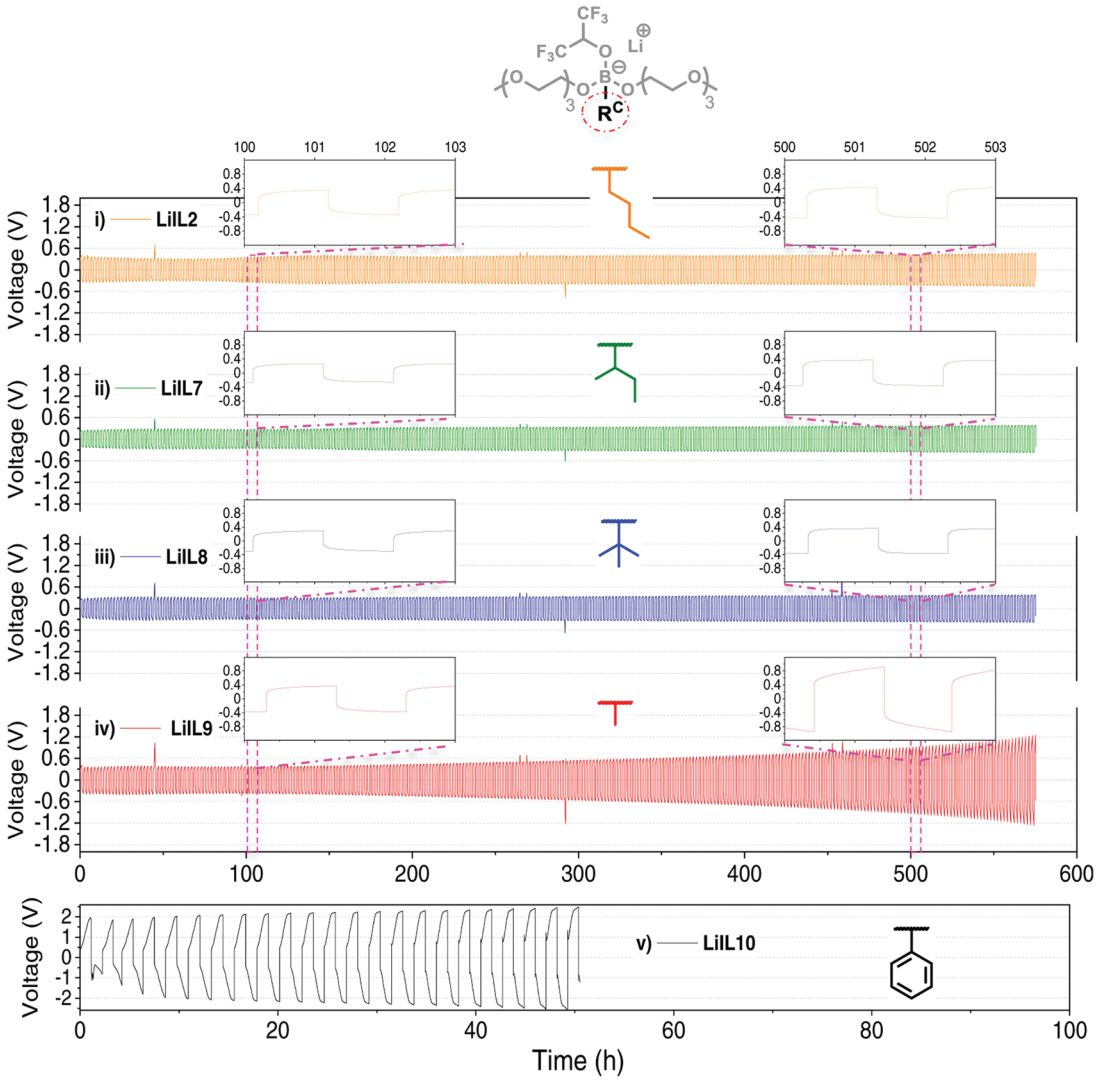

Figure 6. Electrochemical behavior of Li^0 electrode in the as-prepared LiILs. Galvanostatic cycling of $Li^0/LiILs/Li^0$ symmetric cells at 0.2 mA cm^{-2} (half-cycle time 1 h) at 40 °C.

symmetric cells assembled with the LiIL2, LiIL7, and LiIL8 electrolytes withstood cycling for more than 570 h, maintaining extremely stable polarization profiles, demonstrating high reversibility of lithium plating/stripping cycling in these electrolytes. Despite the lower ionic conductivity of the LiIL9 electrolyte, while it supported stable cycling until about 200 h; thereafter the cell overpotential gradually increased from ±0.4 to ±1.1 V versus Li^0/Li^+ after 570 h, demonstrating limited compatibility with lithium electrodes in the long term.

On the other hand, although the ionic conductivity values of the LiIL9 and LiIL10 electrolytes are comparable, the overpotential values in the symmetrical Li^0/LiIL10/Li^0 symmetrical cell >±1.2 V versus Li^0/Li^+ from the initial cycle which is clear evidence of the limited compatibility the of the LiIL10 electrolyte with lithium-metal electrodes. This was associated with generation of side reactions derived from the reactivity of the phenyl group with lithium metal.[33,34]

Subsequently, to analyze the effect of temperature on the long-term cycling stability, additional Li^0/LiILs/Li^0 symmetrical cells with fiberglass spacers (≈100 µm of thickness) were assembled with LiIL2, LiIL7, and LiIL8 electrolytes and cycled at a constant current density of 0.2 mA cm^{-2} at 65 °C (Figure S5, Supporting Information). As expected, the increase in the cycling temperature generated a decrease in the overpotential during the first cycles. However, after the first 50 h, all cells exhibited a gradual increase in overpotential. Particularly, the cells assembled with LiIL2 and LiIL8 electrolytes exhibited overpotential values higher than ±0.9 V versus Li^0/Li^+ after 210 and 910 h, respectively. On the other hand, the cell assembled with LiIL7 electrolyte maintained its overpotential values below ±0.4 V versus Li^0/Li^+ after 1000 h. These results showed that the *sec*-butyl group as a stabilizer increases the compatibility of LiILs with lithium-metal electrodes.

2.5. Electrochemical Performance of LiILs as a Single-Component Electrolyte in Batteries

The previous results determined that the LiIL7 electrolyte presented the best characteristics to be further tested in lithium-metal batteries in combination with inorganic materials. For this reason, the LiIL7 electrolyte was tested in Li^0/LiIL7/cathode cells, using as two well-known active materials with different intercalation chemistries: LFP known as cathode material and LTO known as anode material, which show redox potentials of 3.4 and 1.6 V versus Li^0/Li^+, respectively (**Figure 7**).

The charge/discharge profiles obtained for the Li^0/LiIL7/LFP cell in a potential range of 3.8–2.8 V versus Li^0/Li^+ at a *C*-rate of 0.1 C at 40 °C (Figure S6, Supporting Information) presented a large hysteresis (250 mV) between potentials of 3.35 and 3.5 V versus Li^0/Li^+ associated with the Li^+ intercalation and de-intercalation processes at the LFP electrodes, respectively, due to the limited conductivity of the *sec*-LLS2 electrolyte at the cycling temperature. It was also possible to appreciate that the charge profiles were accompanied by two oxidation stages in the high charge state region: the first one from 3.5 to 3.65 V versus Li^0/Li^+ characteristic of diffusion-limited Li^+ de-intercalation processes in the LFP active material, while the second stage from 3.65 to 3.8 V versus Li^0/Li^+ associated with a large decomposition of the LiIL7 electrolyte, favored by the limited current density applied for cycling. Nevertheless, high and constant discharge density values of 94 mAh g^{-1} were collected for 30 cycles.

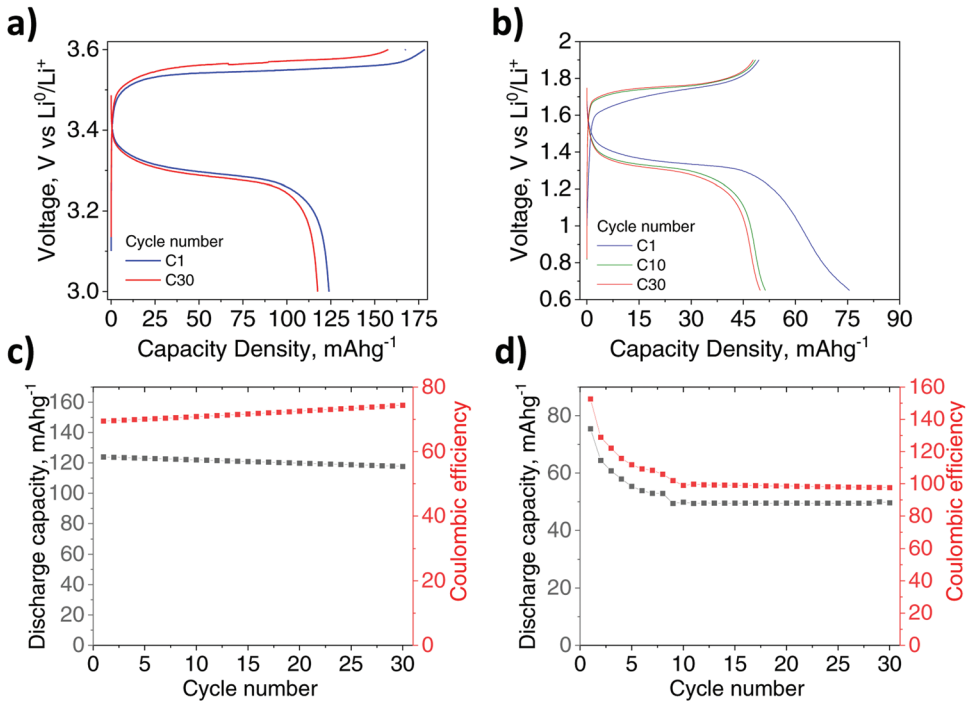

Figure 7. Cycling performance for lithium-metal battery cells based on LiIL7 electrolyte at a *C*-rate of 0.2 C at 65 °C. Charge/Discharge profiles a) Li^0/LiIL7/LFP and b) Li^0/LiIL7/LTO cells cycling stability for c) Li^0/LiIL7/LFP and d) Li^0/LiIL7/LTO cells.

Subsequently, to overcome the limitations identified in the first test, a new Li^0/LiIL7/LFP cell was cycled over a bounded potential range of 3.6–3.0 V versus Li^0/Li^+ at a *C*-rate of 0.2 C at 60 °C (Figure 6a). The charge/discharge profiles collected for this cell showed that, despite the increase in cycling temperature, the hysteresis of the overpotential increased to 50 mV due to the increase in current density. Despite the existence of a large cell activation overpotential, and the poor Coulombic efficiency of 80%, it was possible to collect stable charge and discharge values of 172 and 124 mAh g^{-1}, respectively, with a loss capacity of 5% after 20 cycles (Figure 6c). Finally, the LiIL7 electrolyte was tested in a Li^0/LiIL7/LTO cell cycled in a bounded potential range of 1.9–0.6 V versus Li^0/Li^+ at a *C*-rate of 0.2 C at 60 °C (Figure 6b) the charge/discharge profiles collected for this cell present a hysteresis (250 mV) similar to that obtained for the LFP cathode cell. The charge capacity of 50 mAh g^{-1} for the first cycle remained relatively constant by decreasing 4% from its initial value after 30 cycles (Figure 6d). On the other hand, during the cell stabilization process, the discharge capacity values present relatively high values with respect to the charge capacity values,[11] which is reflected in the unusual Coulombic efficiency.[35–37] However, the discharge capacities gradually decrease during the first nine cycles from 76 to 50 mAh g^{-1} and remain constant during the following cycles.

3. Conclusions

In this article, we investigated a new family of ionic liquid borate—lithium salts at room temperature as a single-component electrolyte for lithium batteries. The design concept of this class of LiILs is based on the combination of a central tetracoordinate boron atom asymmetrically substituted with two oligoethylene glycol units, one fluorinated electron-attracting groups and one alkane group. The new family of borate—Li^+ LiILs showed high ionic conductivity values (>10^{-4} S cm^{-1} at RT), lithium transference numbers (t_{Li^+} = 0.4–0.5) and electrochemical stability(>4 V). We identified the right balance between the electron-withdrawing capacity of the fluorinated groups, the solvating capacity of the ethoxide groups, and the interfacial compatibility of the stabilizing aliphatic groups (B—C bond). Due to its high ionic conductivity, the LiILs showed high compatibility with lithium-metal electrodes with stable polarization profiles in platting/stripping tests. Those LiILs were successfully tested for the first time as single-component electrolytes in lithium-metal batteries showing discharge capacity values in Li^0/LiILs/LFP and Li^0/LiILs/LTO cells of 124 and 75 mAh g^{-1}, respectively, at a *C*-rate of 0.2 C and 65 °C with a low-capacity loss.

Supporting Information

Supporting Information is available from the Wiley Online Library or from the author.

Acknowledgements

This work was funded and supported by a Grant for Basque Government through grant IT1309-19, and European Commission's funded Marie Skłodowska–Curie project POLYTE-EID (Project No. 765828) and Spanish MCIN/AEI/PID2020-119026GB-I00. G.G.-G. is grateful to "Secretaría de Educación, Ciencia, Tecnología e Innovación" from Ciudad de México for the postdoctoral fellowship through grant SECTEI/133/2019. G.G.-G. also thanks the PhD. IOSM for being the driving force and constant support.

Conflict of Interest

The authors declare no conflict of interest.

Authors Contribution

G.G.-G. performed the LiILs' synthesis, structural and electrochemical characterization, and wrote the original draft. M.A.-T. performed electrochemical characterization. J.L.O.-M. performed electrochemical characterization. M.L.P. performed the rheological test. M.F. proposed the topic and corrected the original draft, and D.M. supervised the topic of the work of G.G.-G. and corrected the original draft.

Data Availability Statement

The data that support the findings of this study are available on request from the corresponding author. The data are not publicly available due to privacy or ethical restrictions.

Keywords

borate salts, electrolytes, lithium batteries, lithium ionic liquids

Received: August 31, 2022
Revised: October 5, 2022
Published online: November 6, 2022

[1] S.-P. Chen, D. Lv, J. Chen, Y.-H. Zhang, F.-N. Shi, *Energy Fuels* **2022**, *36*, 1232.
[2] L. Porcarelli, A. S. Shaplov, M. Salsamendi, J. R. Nair, Y. S. Vygodskii, D. Mecerreyes, C. Gerbaldi, *ACS Appl. Mater. Interfaces* **2016**, *8*, 10350.
[3] G. Guzmán-González, H. J. Ávila-Paredes, E. Rivera, I. González, *ACS Appl. Mater. Interfaces* **2018**, *10*, 30247.
[4] J. Wang, S. Li, Q. Zhao, C. Song, Z. Xue, *Adv. Funct. Mater.* **2021**, *31*, 2008208.
[5] G. Guzmán-González, S. Vauthier, M. Alvarez-Tirado, S. Cotte, L. Castro, A. Guéguen, N. Casado, D. Mecerreyes, *Angew. Chem., Int. Ed.* **2022**, *61*, e202114024.
[6] R. Klein, O. Zech, E. Maurer, M. Kellermeier, W. Kunz, *J. Phys. Chem. B* **2011**, *115*, 8961.
[7] N. Karimi, M. Zarrabeitia, M. Hosseini, T. Ates, B. Iliev, T. J. S. Schubert, A. Varzi, S. Passerini, *ACS Appl. Mater. Interfaces* **2022**, *14*, 20888.
[8] K. Kubota, H. Matsumoto, *J. Phys. Chem. C* **2013**, *117*, 18829.
[9] B. B. Hallac, O. E. Geiculescu, R. V. Rajagopal, S. E. Creager, D. D. DesMarteau, *Electrochim. Acta* **2008**, *53*, 5985.
[10] X. Wang, F. Chen, G. M. A. Girard, H. Zhu, D. R. MacFarlane, D. Mecerreyes, M. Armand, P. C. Howlett, M. Forsyth, *Joule* **2019**, *3*, 2687.
[11] J. Sakuda, E. Hosono, M. Yoshio, T. Ichikawa, T. Matsumoto, H. Ohno, H. Zhou, T. Kato, *Adv. Funct. Mater.* **2015**, *25*, 1206.
[12] T. Fujinami, Y. Buzoujima, *J. Power Sources* **2003**, *119–121*, 438.

[13] H. Shobukawa, H. Tokuda, S.-I. Tabata, M. Watanabe, *Electrochim. Acta* **2004**, *50*, 305.
[14] E. Zygadło-Monikowska, Z. Florjańczyk, J. Ostrowska, P. Bołtromiuk, J. Frydrych, W. Sadurski, N. Langwald, *Electrochim. Acta* **2011**, *57*, 66.
[15] E. Zygadło-Monikowska, Z. Florjańczyk, K. Służewska, J. Ostrowska, N. Langwald, A. Tomaszewska, *J. Power Sources* **2010**, *195*, 6055.
[16] E. Zygadło-Monikowska, Z. Florjańczyk, A. Tomaszewska, M. Pawlicka, N. Langwald, R. Kovarsky, H. Mazor, D. Golodnitsky, E. Peled, *Electrochim. Acta* **2007**, *53*, 1481.
[17] M. B. Herath, S. E. Creager, R. V. Rajagopal, O. E. Geiculescu, D. D. DesMarteau, *Electrochim. Acta* **2009**, *54*, 5877.
[18] D. Flachard, J. Rolland, M. M. Obadia, A. Serghei, R. Bouchet, E. Drockenmuller, *Chem. Commun.* **2018**, *54*, 9035.
[19] G. Guzmán-González, G. Ramos-Sánchez, L. E. Camacho-Forero, I. González, *J. Phys. Chem. C* **2019**, *123*, 17686.
[20] Y. Sun, G. Li, Y. Lai, D. Zeng, H. Cheng, *Sci. Rep.* **2016**, *6*, 22048.
[21] B. Roy, P. Cherepanov, C. Nguyen, C. Forsyth, U. Pal, T. C. Mendes, P. Howlett, M. Forsyth, D. MacFarlane, M. Kar, *Adv. Energy Mater.* **2021**, *11*, 2101422.
[22] P. Jankowski, W. Wieczorek, P. Johansson, *Phys. Chem. Chem. Phys.* **2016**, *18*, 16274.
[23] J. Clarke-Hannaford, M. Breedon, T. Rüther, M. J. S. Spencer, *Nanomaterials* **2021**, *11*, 2391.
[24] D. R. MacFarlane, M. Forsyth, E. I. Izgorodina, A. P. Abbott, G. Annat, K. Fraser, *Phys. Chem. Chem. Phys.* **2009**, *11*, 4962.
[25] Y. Wang, F. Fan, A. L. Agapov, X. Yu, K. Hong, J. Mays, A. P. Sokolov, *Solid State Ionics* **2014**, *262*, 782.
[26] K. Ueno, H. Tokuda, M. Watanabe, *Phys. Chem. Chem. Phys.* **2010**, *12*, 1649.
[27] J. Evans, C. A. Vincent, P. G. Bruce, *Polymer* **1987**, *28*, 2324.
[28] K. Yoshida, M. Nakamura, Y. Kazue, N. Tachikawa, S. Tsuzuki, S. Seki, K. Dokko, M. Watanabe, *J. Am. Chem. Soc.* **2011**, *133*, 13121.
[29] G. G. Eshetu, X. Judez, C. Li, M. Martinez-Ibañez, I. Gracia, O. Bondarchuk, J. Carrasco, L. M. Rodriguez-Martinez, H. Zhang, M. Armand, *J. Am. Chem. Soc.* **2018**, *140*, 9921.
[30] D. Di Lecce, V. Marangon, H.-G. Jung, Y. Tominaga, S. Greenbaum, J. Hassoun, *Green Chem.* **2022**, *24*, 1021.
[31] W. Xu, L.-M. Wang, R. A. Nieman, C. A. Angell, *J. Phys. Chem. B* **2003**, *107*, 11749.
[32] P. H. Figueiredo, L. J. A. Siqueira, M. C. C. Ribeiro, *J. Phys. Chem. B* **2012**, *116*, 12319.
[33] W. Li, *J. Electrochem. Soc.* **2020**, *167*, 090514.
[34] J. Kalhoff, G. G. Eshetu, D. Bresser, S. Passerini, *ChemSusChem* **2015**, *8*, 2154.
[35] M. Odziomek, F. Chaput, A. Rutkowska, K. Świerczek, D. Olszewska, M. Sitarz, F. Lerouge, S. Parola, *Nat. Commun.* **2017**, *8*, 15636.
[36] A. Laumann, M. Bremholm, P. Hald, M. Holzapfel, K. T. Fehr, B. B. Iversen, *J. Electrochem. Soc.* **2011**, *159*, A166.
[37] M. Ding, H. Liu, X. Zhao, L. Pang, L. Deng, M. Li, *RSC Adv.* **2017**, *7*, 43894.